Chapter

Raman Features of Linear-Carbon-Chain and Multiwall Carbon Nanotube Composites

Yahachi Saito and Koji Asaka

Abstract

Structural and electronic properties of multiwall carbon nanotubes (MWCNTs) containing linear carbon chains (LCCs), which were produced by arc-discharge between carbon electrodes in an atmospheric pressure, have been studied by Raman spectroscopy as well as electron microscopy. Spectral features of Raman scattering from the LCC/MWCNT composites were reviewed with emphasis on the spectra obtained with a low energy photon (1.58 eV, 785 nm) excitation, which have not been described in detail so far. Characteristic frequencies of LCC stretching modes with the 785 nm laser excitation are observed at around 1740, 1759, and 1789 cm^{-1}. In a low frequency region, radial breathing modes (RBMs) of the innermost tube within MWCNTs are observed at specific frequencies of 293, 341, 402, and 510 cm^{-1}; the highest RBM frequency is tentatively assigned to a tube with the chiral index (4,3), whose diameter is expected to 0.50 nm. LCC bands observed with various excitation wavelengths from 488 to 785 nm show that the band consists of several peaks, and the relative intensities of constituent peaks change with the excitation wavelengths due to the resonance effect; the higher the excitation photon energy is, the higher the intensity of high-frequency LCC modes.

Keywords: carbyne, linear carbon chain, carbon nanotube, Raman, resonance

1. Introduction

Carbon exists in a variety of allotropes: e.g., diamond, graphite, fullerene, and carbon nanotube (CNT). Besides these well-known allotropes, carbyne, an infinite carbon chain, has attracted much interest with significant controversy since the late 1960s [1–5]. Linear carbon chains (LCCs) in its own forms are unstable in an ambient environment. In solution, LCCs up to $C_{12}H_2$ are formed [6]. When both ends of carbon chains are anchored by bulky molecules, polyyne consisting of carbon atoms up to 44 have so far been chemically synthesized [7, 8]. Recently, LCCs confined inside CNTs have been discovered in multiwall CNT (MWCNT) produced by arc discharge [9], in high-temperature annealed double-wall CNTs (DWCNT) [10], and in single-wall CNT (SWCNT) suffered from electric discharge [11]. The structural and electronic properties of the encapsulated LCCs have been mainly measured by transmission electron microscopy (TEM) and

Raman scattering spectroscopy, and it has been revealed that the length of LCC inside CNTs exceeds 30 nm (i.e., more than 230 carbon atoms).

LCC corresponds to a long polyyne with effectively infinite length, in which the sp-hybridized orbitals form alternated single and triple bonds between carbon atoms in the one-dimensional (1D) chain, and thus an electronic band gap is open at the Fermi level. The electronic energy gap of hydrogen-capped polyynes $C_{2m}H_2$ is expected to be in a range from 4.1 eV for $2m = 8$ to 2.2 eV for an infinitely long polyyne [12]. Reflecting the energy gap in 1D materials, strong resonance Raman scatterings are expected. Actually, Raman scattering characteristic to LCC (called "LCC bands") has been observed from 1750 to 1855 cm^{-1}, depending on incident photon energies (1.6–2.6 eV). The LCC bands originate from one-dimensional stretching vibration of triple-bonded carbon atoms [6, 13–15].

Raman spectroscopy is a powerful and effectual technique to characterize nano-carbon materials including LCC and CNT. In measuring LLCs encapsulated in CNTs by Raman, the wavelengths of incident lasers employed so far were mainly in a visible region [9, 10, 16–18], because strong scatterings from LCCs are observed owing to resonance Raman. In this report, focusing to Raman spectra obtained with a long wavelength (near infrared) incident laser of 785 nm, which have not been reported in detail so far, characteristic features of LCC bands and radial breathing modes of MWCNTs at various incident wavelengths (785, 633, 532 and 488 nm) are presented. The materials studied here is MWCNTs encapsulating LCCs, which were produced by carbon arc-discharge being blown with inactive gases in the atmosphere [19].

2. MWCNT encapsulating LCC prepared by arc discharge

MWCNTs encapsulating LCC were synthesized by arc-discharge between carbon electrodes in the atmospheric pressure. The LCC/MWCNT composite materials investigated in the present study was supplied from JFE Engineering Corporation. The details of the production procedure have been described in the public patent documents [19]. Briefly, the anode is a hollow carbon rod (outer diameter 10 mm, inner diameter 4 mm), and the cathode is a fat carbon rod (diameter 35 mm) which executes a motion of rotation around its axis (1.5 rotation/min), as shown in **Figure 1(a)**. The anode translates (35 mm/min) parallel to the axis of the cathode, keeping a gap between the anode end and the cathode surface constant (ca. 1 mm). Arc discharging (DC 100A, 20 V) was fired in the gap between the anode and the
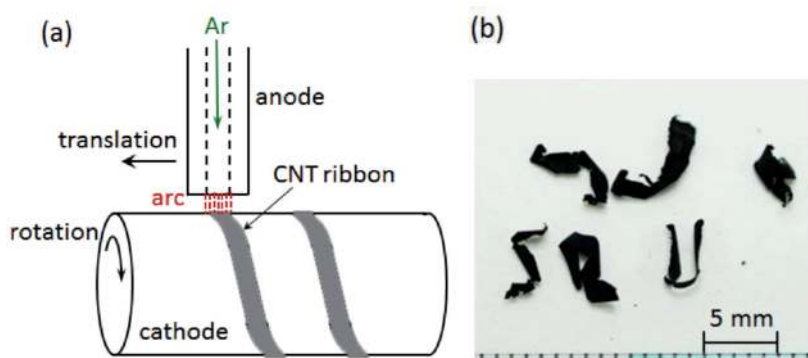

Figure 1.
(a) Schematic diagram of an arc-discharge apparatus for MWCNT production, and (b) photograph of produced ribbons consisting of MWCNT encapsulating LCC.

cathode. During the discharge, Ar gas was flowed through the inner hole of the anode toward the arcing gap, and also a cooling gas (e.g., N_2) was blown to the gap in order to cool and remove carbonaceous deposits formed on the cathode surface. The carbon deposit produced after the discharge had a form of thin tape (2–5 mm wide, and 10–20 μm thick) as shown in **Figure 1(b)**.

3. Surface morphology observed by SEM

As shown later by micro-Raman spectroscopy, in a tape of LCC/MWCNT composite, there are two types of regions; one contains abundant LCCs while the other scarce LCCs. Hereafter, the former region is called the "A" region, and the latter the "B" region. The surface morphology of the MWCNT tape at various places are observed by a scanning electron microscope (SEM) using a ThermoFisher Prisma-E operated at 15–20 kV. **Figure 2(a)** and **(b)** show SEM images of surfaces of the "A" and "B" regions, respectively. In both regions, abundant MWCNTs are observed, and no outstanding difference between the SEM images is apparently found. By close-inspection, however, the surface of the "A" region (**Figure 2(a)**) is found to be rugged and show a blanket-like surface, while the "B" region (**Figure 2(b)**) looks smooth and contains small particles (possibly, carbon nanoparticles).
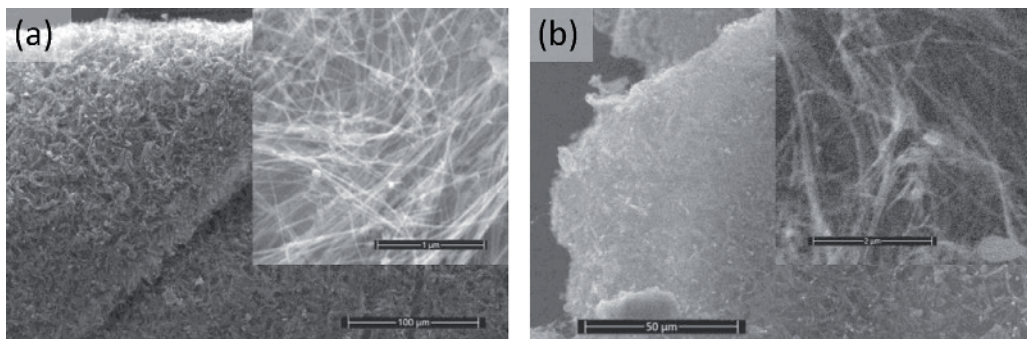

Figure 2.
SEM images of (a) the area "A" with the blanket-like surface morphology and (b) the area "B" with smooth appearance. Insets show high magnification images of each area.
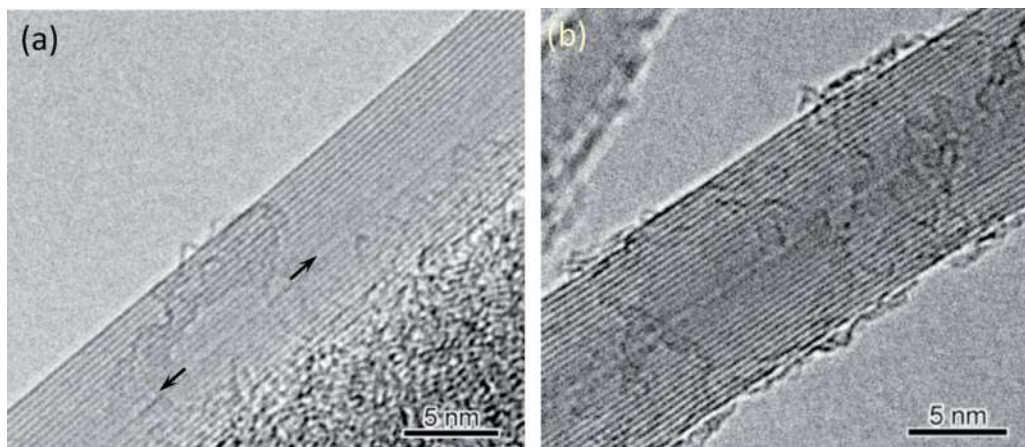

Figure 3.
TEM images of (a) MWCNT encapsulating LCCs inside the innermost tube, and (b) MWCNT with the empty innermost tube with diameter of ca. 0.47 nm. Arrows in (a) point LCCs encapsulated in the core of the MWCNT.

4. TEM observation of LCC encapsulated in MWCNT

Transmission electron microscopy (TEM) was also performed to investigate the detailed inner structure of MWCNTs encapsulating LCCs by using a JEOL JEM-2010 operated at 120 kV. The TEM samples were prepared by dropping MWCNTs dispersed in isopropyl alcohol onto a microgrid for TEM. The diameter of individual MWCNTs is in a range from 7 to 20 nm, as revealed by high resolution transmission electron microscopy, and the length exceeds 1 µm. **Figure 3(a)** shows a MWCNT encapsulating a LCC inside the innermost tube. Arrows point LCCs encapsulated in the core of the MWCNT. The length of the LCC is over 20 nm, and the diameter of the innermost tube is about 0.7 nm. **Figure 3(b)** shows a MWCNT with an empty innermost tube with diameter of ~ 0.47 nm. The innermost diameters in the present sample is smaller than those (4–10 nm) of ordinary MWCNTs [20] prepared by other methods, e.g., ordinary arc-discharge in He gas, catalyst-assisted thermal decomposition of hydrocarbon gases and so on.

5. Raman spectra of LCC/MWCNT composite at different excitation lasers

Raman spectroscopy was carried out using a Renishaw inVia confocal Raman microscope with 488, 532, 633, and 785 nm excitation lasers. A piece of the LCC/MWCNT composite tape adhered to an Al plate was placed on the microscope stage, and Raman spectra were measured at room temperature. Objective lenses employed were mainly 50× and 20×, and the spot size of laser on a sample was approximately 1 µm. Laser power on sample surfaces was in a range from 0.2 to 3.0 mW for 488, 532, and 633 nm, and in a range from 0.25 to 5.2 mW for 785 nm.

Typical Raman scattering spectra from the region "A" of the LCC/MWCNT composite obtained with four different excitation lasers, 488, 532, 633, and 785 nm are shown in **Figure 4**. In addition to D and G bands, strong peaks at higher frequencies (1750–1850 cm^{-1}) labeled LCC, attributed to stretching vibrations of triple bonds in one-dimensional carbon chains, are observed; the peak height is much stronger than the G-band for 488, 532, and 633 nm excitations. The enhanced peaks of LCC are attributed to resonance of the band gaps of LCCs with the incident photon energies.

A band of LCC observed from the tape-shaped sample (coagulated dense sample) is relatively wide in frequency (~50 cm^{-1}) and exhibits multiple peaks and/or shoulders, as found conspicuously in **Figure 4(b)** and **(c)**. Micro-Raman investigation of a finely dispersed thin sample showed that only one peak with a narrow FWHM (full width at half-maxima) of about 10 cm^{-1} was observed [21] when one or a few MWCNTs containing a LCC were shined by a focused incident laser.

In a low frequency region (< 600 cm^{-1}), radial breathing modes (RBMs) are clearly observed even for MWCNTs. RBM, whose frequency is inversely proportional to the diameter of CNT [22], is a characteristic signature for SWCNT and thin DWCNT, but even MWCNT shows this mode when the inner-most tube in it is extremely small, e.g., less than 1 nm [23]. Observable RBM frequencies depend on the excitation photon energies; CNTs which are in resonance with the incident photon energy (i.e., when optically-allowed transition gaps between van Hove singularities match with the photon energy) expose RBM peaks in Raman spectra. **Figure 5** shows a Raman spectrum extending up to 6000 cm^{-1} with the 532 nm
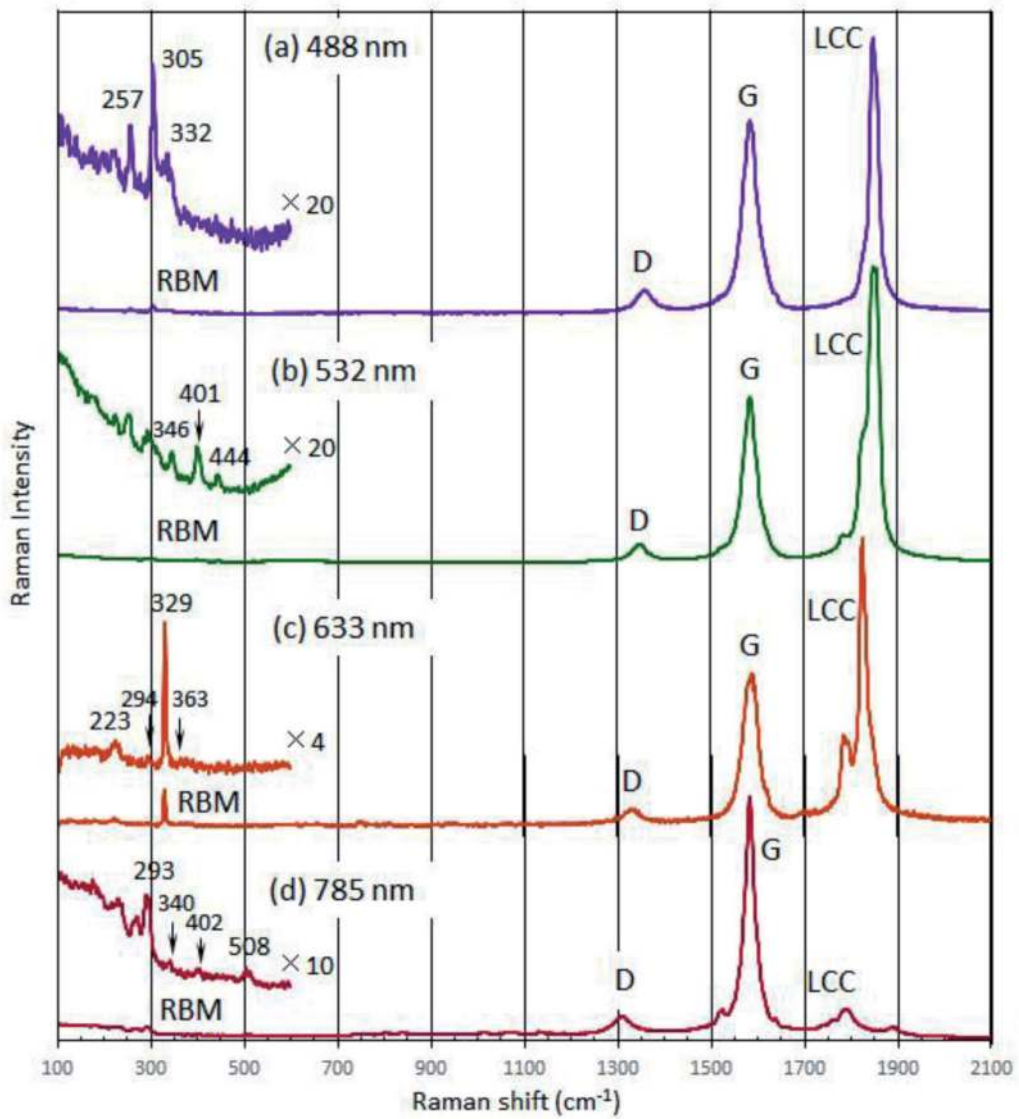
Figure 4.
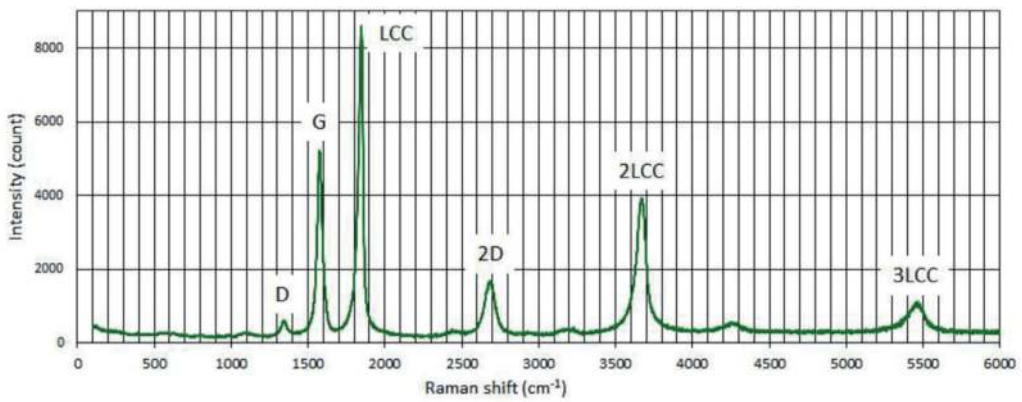*Raman scattering spectra of LCC@MWCNT composite with 488, 532, 633, and 785 nm laser excitations.*

Figure 5.
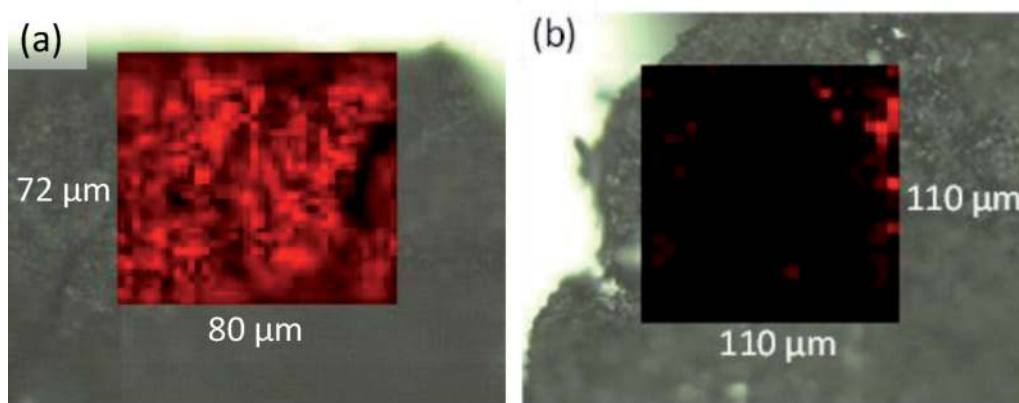*Raman spectrum showing overtones of LCC with 532 nm laser excitation.*

5

Figure 6.
Raman mappings of the LCC band (1790–1890 cm^{-1}) with 532 nm excitation in the areas (a) "A" and (b) "B". the brighter red corresponds to the stronger LCC band.

excitation, exhibiting overtones of the LCC band. Appearance of the strong 2nd and 3rd overtones, being labeled "2LCC" and "3LCC", respectively, indicates the resonance of LCCs with the incident photon energy.

Figure 6(a) and **(b)** show Raman mappings of the LCC bands with the 532 nm excitation in the areas "A" and "B", respectively. In the area "A", as shown in **Figure 6(a)**, the distribution of LCCs is relatively uniform, revealing the presence of LCCs over the area. In the area "B" (**Figure 6(b)**), on the other hand, the LCC peaks are rarely observed.

6. Raman scattering from the near-infrared 785 nm laser

As shown in **Figure 4**, the intensity of LCC band for the 785 nm excitation is much low compared to those for the shorter wavelength excitations. This may be owing to the weak resonance with this long wavelength (or low photon energy) laser. Electronic band gaps of LCCs depend on their lengths; the longer the length of LCCs is, the narrower the electronic energy gap of the LCC [12], suggesting that the population of long LCCs whose energy gaps match with the 785 nm (1.58 eV) laser in the present sample is much lower than those of shorter LCCs which resonate with the other shorter wavelength (633, 532, and 488 nm) lasers.

In Raman spectra from ordinary CNTs (i.e., no LCC inside) excited at 785 nm laser, weak peaks appear in a region from 1700 to 1900 cm^{-1}, which were assigned to an overtone of out-of-plane transversal optical mode (2oTO) and a combination mode of in-plane TO and longitudinal acoustic modes (iTO+LA) [24]. The vibrational frequencies of these modes show a dispersion (i.e., the frequencies change with the incident wavelength) and fall in a region of LCC modes at 785 nm excitation, as shown in **Figure 7**. The spectrum in **Figure 7(a)** is obtained from a LCC abundant region (A), and that in **Figure 7(b)** from a LCC-absent region (B). The peak at 1889 cm^{-1} in **Figure 7(a)** is considered to originate from the iTO+LA mode of carbon nanotubes, because the vibration frequency (1889 cm^{-1}) is too high for the LCCs. Concerning the peak at 1789 cm^{-1}, a large portion of its intensity come from the 2oTO mode of carbon nanotubes, but there may be some contribution from LCCs because the peak height (relative to that of iTO+LA) in **Figure 7(a)** is apparently higher than that in **Figure 7(b)**. Fine peaks and shoulders, which are absent in **Figure 7(b)**, are observed in **Figure 7(a)**. These additional peaks/shoulders are signals from LCCs.
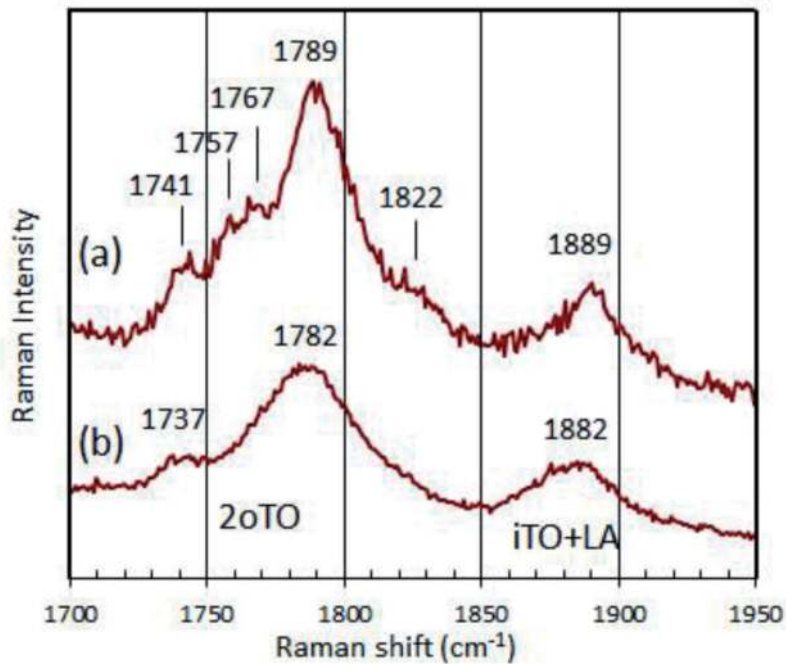
Figure 7.
Raman spectra in a LCC frequency range from (a) LCC-abundant and (b) LCC-absent regions with the 785 nm excitation.

7. Observable LCC vibration modes changing with the incident photon energies

Figure 8 shows a diagram displaying the observed Raman frequencies and intensities of LCC bands as a function of the incident photon energy. A tendency that the LCC frequency becomes lower with the decrease of the excitation photon energy is found; the observed LCC frequencies distribute from 1740 to 1820 cm^{-1}
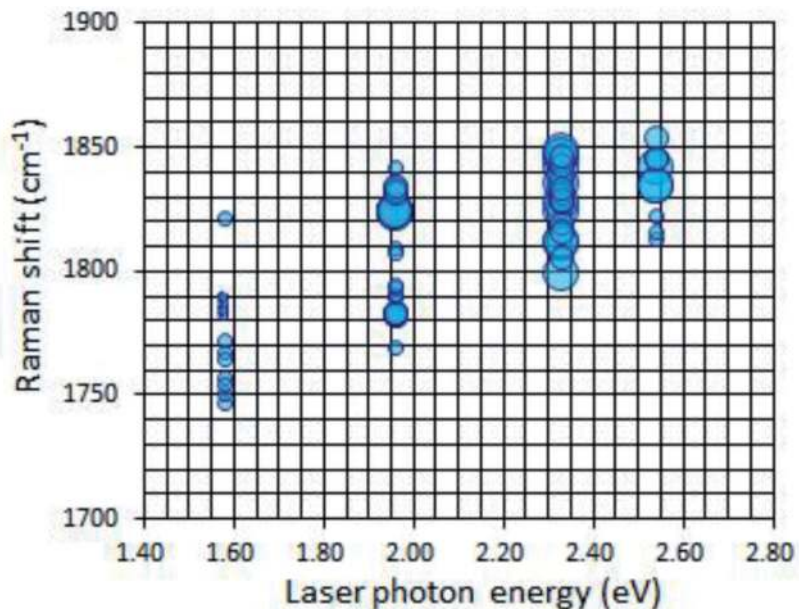

Figure 8.
LCC peak positions and intensity versus excitation energy. Size of circles represents roughly the intensity of LCC peaks; larger circles show higher intensity.

for the lowest photon energy 1.58 eV (785 nm), from 1770 to 1840 cm^{-1} for 1.96 eV (633 nm), from 1800 to 1850 cm^{-1} for 2.33 eV (532 nm), and concentrate to a band from 1810 and 1855 cm^{-1} for the highest photon energy 2.54 eV (488 nm). The change of LCC frequencies with the excitation photon energy is caused by the resonance of the energy gaps of LCCs with the incident photon. The vibrational frequency as well as the energy gap of LCC depends on its length [12, 25]; the longer the length is, the lower the vibrational frequency and the narrower the energy gap are. Lower-energy photons resonate with the longer LCCs and manifest lower-frequency vibrational modes. The incident photon dependence suggests that the energy gaps of LCCs in the present sample extend from 1.58 eV to at least 2.54 eV. The local environment inside a CNT is expected to modify the vibrational frequency as well as the energy gap due to the interaction between the LCC and CNT walls. At present, the effects of CNT hosts on the energy gap and the vibrational frequency of LCCs as a function of the LCC length are not thoroughly known, though the shifts in the band gap and the chain mode frequency depending on the diameter and the chirality of CNT hosts are reported [26].

8. Raman spectra of LCC/MWCNT composite with 785 nm excitation at different laser powers

Figure 9 shows Raman spectra obtained with the 785 nm excitation at different incidence powers from 0.25 to 5.2 mW. Broadening of the peaks and thus burring/disappearance of fine structures in the G and LCC bands are obviously discerned with the increase of incidence laser power. At low powers, satellite peaks (1520 and
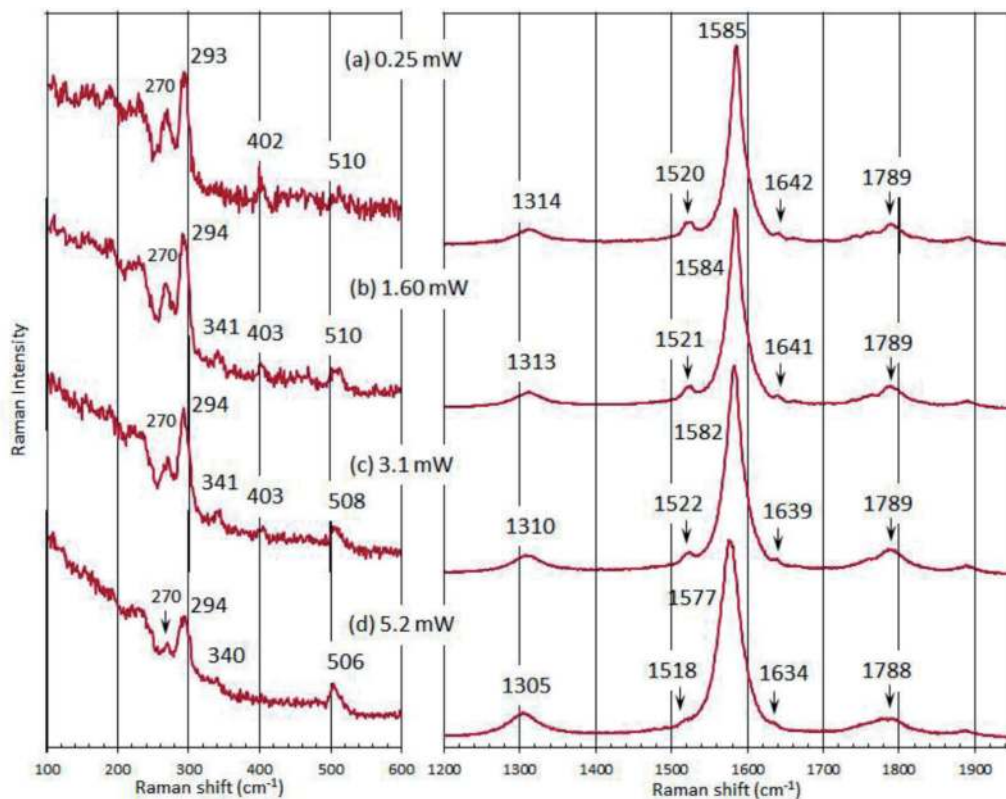

Figure 9.
Raman spectra in a low frequency RBM region and in a high frequency region including D, G and LCC bands (1200–1950 cm^{-1}) with 785 nm excitation at different incident laser powers.

1642 cm^{-1}) on both sides of the G-peak are clearly observed. These satellites are not identified yet. To the best of the authors' knowledge, no reports on the assignment of these satellites are found. Possibility of any combination modes of the G and the shear (a telescope and a rotary mode for MWCNT, 49 and 58 cm^{-1}, respectively [27]) should be accessed in the future study.

The peaks of the D and G bands shift to lower frequencies with the increase of laser power, as shown in **Figure 10(a)** and **(b)**, respectively. The shifts of these modes are caused by the temperature rise owing to the incidence laser. According to the previous report on the temperature dependence of the G-band frequencies of CNTs [28], the temperatures of the LCC/MWCNT sample shined by the 785 nm laser are estimated to be room temperature, 320 K, 400 K, and 610 K for **Figure 9(a)–(d)**, respectively. The temperature dependence of LCC and RBM frequencies is weak in this temperature range, as shown in **Figure 10(c)** and **(d)**.

In the low frequency region of **Figure 9**, radial breathing modes (RBMs) are observed even for MWCNTs. RBMs are commonly observed for SWCNTs (with diameter d less than ~ 1.5 nm) [29] and DWCNTs with a small inner CNT (d < ~ 1 nm) [30], but the ordinary MWCNTs whose innermost tube is large, typically 4–10 nm, do not exhibit RBMs. The appearance of RBM in the present MWCNTs indicates the presence of small tubes (d < 1 nm) in the core of MWCNTs [23]. RBMs at 402 and 510 cm^{-1} observed in **Figure 9** suggest the presence of extremely small core-tubes with diameters 0.63 and 0.50 nm, respectively, according to the relation between the RBM frequency ν_R and the diameter, $\nu_R = 254/d$ [31]. The smallest tube
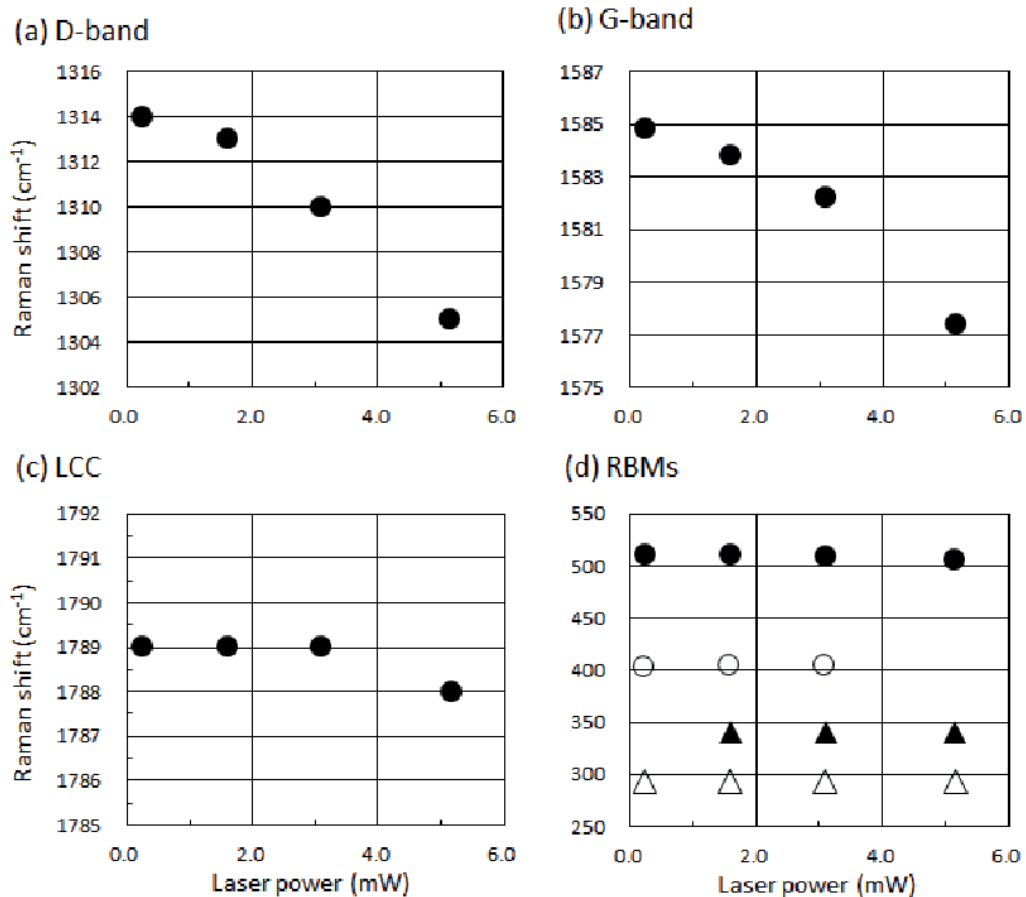

Figure 10.
Peak frequencies of (a) D, (b) G, (c) LCC, and (d) RBMs at 294, 341, 403, and 510 cm^{-1} as a function of the irradiating laser power.

giving the highest RBM of 510 cm^{-1} is tentatively assigned to the tube with a chiral index (4,3). The diameters estimated from Raman are consistent with the TEM observation, as shown in **Figure 3**.

9. Conclusions

Multiwall carbon nanotubes (MWCNTs) consisting of several to ten-something walls, which were produced by carbon arc-discharge in the atmospheric pressure with blowing inactive gases, contain long linear carbon chains (LCCs) whose length exceeds 20 nm. Signatures of LCCs in Raman scattering appear at a high frequency region from 1740 to 1855 cm^{-1}, depending on the wavelength of incident lasers. The longer the wavelengths of excitation lasers are, the lower the observed LCC frequencies are. Visible light lasers (633, 532, and 488 nm) show strong LCC-bands due to resonance Raman scattering. Even the 785 nm laser exhibits LCC signatures in a frequency range from 1740 to 1820 cm^{-1}, though their intensities are low. The incident photon-energy dependence signifies the energy gaps of LCCs extend from 1.58 eV to at least 2.54 eV. In a low frequency region, RBMs were also observed, indicating the presence of extremely small tubes in the core of MWCNTs. RBMs at 402 and 510 cm^{-1} suggest the diameters of innermost tubes are 0.63 and 0.50 nm, respectively. The diameters estimated from Raman are consistent with the TEM observation.

Acknowledgements

Author details

Yahachi Saito[1*] and Koji Asaka[2]

1 Toyota Physical and Chemical Research Institute, Nagakute, Japan

2 Department of Applied Physics, Nagoya University, Nagoya, Japan

*Address all correspondence to: ysaito@toyotariken.jp

IntechOpen

References

[1] A. El Goresy and G. Donnay, Science 161 (1968) 363-364.

[2] A. G. Whittaker and P. L. Kintner, Science 165 (1969) 589-591.

[3] A. G. Whittaker, Science 200 (1978) 763-764.

[4] P. P. K. Smith and P. R. Buseck, Science 216 (1982) 984-986.

[5] R. B. Heimann, J. Kleiman, and N. M. Salansky, Nature 306 (1983) 164-167.

[6] T. Wakabayashi, H. Tabata, T. Doi, H. Nagayama, K. Okuda, R. Umeda, I. Hisaki, M. Sonoda, Y. Tobe, T. Minematsu, K. Hashimoto, and S. Hayashi, Chem. Phys. Lett. 433 (2007) 296-300.

[7] S. Eisler, A. D. Slepkov, E. Elliott, T. Luu, R. McDonald, F. A. Hegmann, and R. R. Tykwinski, J. Am. Chem. Soc. 127 (2005) 2666-2676.

[8] W. A. Chalifoux and R. R. Tykwinski, Nature Chem. 2 (2010) 967-971.

[9] X. Zhao, Y. Ando, Y. Liu, M. Jinno, and T. Suzuki, Phys. Rev. Lett. 90 (2003) 187401 (4p).

[10] L. Shi, P. Rohringer, K. Suenaga, Y. Niimi, J. Kotakoski, J. C. Meyer, H. Peterlik, M. Wanko, S. Cahangirov, A. Rubio, Z. J. Lapin, L. Novotny, P. Ayala, and T. Pichler, Nature Mater. 15 (2016) 634-640.

[11] S. Toma, K. Asaka, M. Irita and Y. Saito, Surf. Interface Anal. 51 (2019) 131-135

[12] S. Yang and M. Kertesz, J. Phys. Chem. A 110 (2006) 9771-9774.

[13] M. Tommasini, D. Fazzi, A. Milani, M. Del Zoppo, C. Castiglioni, and G. Zerbi, J. Phys. Chem. A 111 (2007) 11645-11651.

[14] N. R. Agarwal, A. Lucotti, D. Fazzi, M. Tommasini, C. Castiglioni, W.A. Chalifoux, and R. R. Tykwinski, J. Raman Spectrosc. 44 (2013) 1398-1410.

[15] M. Jinno, Y. Ando, S. Bandow, J. Fan, M. Yudasaka, and S. Iijima, Chem. Phys. Lett. 418 (2006) 109-114.

[16] L. Shi, P. Rohringer, M. Wanko, A. Rubio, S. Waßerroth, S. Reich, S. Cambré, W. Wenseleers, P. Ayala, and T. Pichler, Phys. Rev. Mater. 1 (2017) 075601 (7p).

[17] Y. Zhang, J. Zhao, Y. Fang, Y. Liu, and X. Zhao, Nanoscale 10 (2018) 17824-17833.

[18] C.-S. Kang, K. Fujisawa, Y.-I. Ko, H. Muramatsu, T. Hayashi, M. Endo, H. J. Kim, D. Lim, J. H. Kim, Y. C. Jung, M. Terrones, M. S. Dresselhaus, and Y. A. Kim, Carbon 107 (2016) 217-224.

[19] Y. Nishi, Japan Patent No. JP3861857B2 (Dec. 27, 2006). Y. Nishi, H. Mukai, and D. Ozamoto, United States Patent No. US7625545B2 (Dec. 1, 2009).

[20] Y. Saito, R. Mizushima, S. Kondo and M. Maida, Jpn. J. Appl. Phys. 39 (2000) 4168-4173.

[21] Unpublished data

[22] J. Kürti, G. Kresse, and H. Kuzmany, Phys. Rev. B 58 (1998) R8869-R8872.

[23] X. Zhao, Y. Ando, L.-C. Qin, H. Kataura, Y. Maniwa, and R. Saito, Chem. Phys. Lett. 361 (2002) 169-174.

[24] V. W. Brar, G. G. Samsonidze, M. S. Dresselhaus, G. Dresselhaus, R. Saito, A. K. Swan, M. S. Ünlü, B. B. Goldberg, A. G. S. Filho, and A. Jorio, Phys. Rev. B 66 (2002) 155418 (10p).

[25] S. Yang, M. Kertesz, V. Zólyomi, and J. Kürti, J. Phys. Chem. A 111 (2007) 2434-2441.

[26] S. Heeg, L. Shi, L. V. Poulikakos, T. Pichler, and L. Novotny, Nano Lett. 18 (2018) 5426-5431.

[27] P. C. Eklund, J. M. Holden, and R. A. Jishi, Carbon 33 (1995), 959-972.

[28] F. Huang, K. T. Yue, P. Tan, S.-L. Zhang, Z. Shi, X. Zhou, and Z. Gu, J. Appl. Phys. 84 (1998), 4022-4024.

[29] S. Bandow, S. Asaka, and Y. Saito, Phys. Rev. Lett. 80 (1998) 3779-3782.

[30] S. Bandow, G. Chen, G. U. Sumanasekera, R. Gupta, M. Yudasaka, S. Iijima, and P. C. Eklund, Phys. Rev. B 66 (2002) 075416 (8p).

[31] G. G. Samsonidze, R. Saito, N. Kobayashi, A. Grüneis, J. Jiang, A. Jorio, S. G. Chou, G. Dresselhaus, M. S. Dresselhaus, Appl. Phys. Lett. 85 (2004) 5703-5705.